Available online at www.sciencedirect.com
ScienceDirect
Catalysis Today 131 (2008) 339–346
CATALYSIS TODAY
www.elsevier.com/locate/cattod

Superior performance of Ir-substituted hexaaluminate catalysts for N_2O decomposition

Shaomin Zhu [a,b], Xiaodong Wang [a], Aiqin Wang [a], Tao Zhang [a,*]

[a] State Key Laboratory of Catalysis, Dalian Institute of Chemical Physics, Chinese Academy of Sciences, Dalian 116023, China
[b] Graduate School of the Chinese Academy of Sciences, Beijing, China

Available online 26 November 2007

Abstract

Novel Ir-substituted hexaaluminate catalysts were developed for the first time and used for catalytic decomposition of high concentration of N_2O. The catalysts were prepared by one-pot precipitation and characterized by X-ray diffraction (XRD), N_2-adsorption, scanning electronic microscopy (SEM) and temperature-programmed reduction (H_2-TPR). The XRD results showed that only a limited amount of iridium was incorporated into the hexaaluminate lattice by substituting Al^{3+} to form $BaIr_xFe_{1-x}Al_{11}O_{19}$ after being calcined at 1200 °C, while the other part of iridium existed as IrO_2 phase. The activity tests for high concentration (30%, v/v) of N_2O decomposition demonstrated that the $BaIr_xFe_{1-x}Al_{11}O_{19}$ hexaaluminates exhibited much higher activities and stabilities than the Ir/Al_2O_3-1200, and the pre-reduction with H_2 was essential for activating the catalysts. By comparing $BaIr_xFe_{1-x}Al_{11}O_{19}$ with $BaIr_xAl_{12-x}O_{19}$ ($x = 0$–0.8), it was found that iridium was the active component in the N_2O decomposition and the framework iridium was more active than the large IrO_2 particles. On the other hand, Fe facilitated the formation of hexaaluminate as well as the incorporation of iridium into the framework.

Keywords: N_2O decomposition; Iridium; Hexaaluminate; Propellant

1. Introduction

The catalytic decomposition of nitrous oxide (N_2O) has received growing interest because of its environmental effect [1]. Most of studies are focused on catalytic decomposition of low concentration of N_2O. Various catalytic systems have been found to be effective for N_2O decomposition, such as supported noble metals [2,3], spinels [4,5], ex-hydrotalcites [6–9] and zeolites [10–12].

However, from another point of view, N_2O is being regarded as a promising green propellant for space propulsion due to its extremely low toxicity compared to traditional hydrazine propellant [13–15]. For this special application, activity is not the only parameter to be considered. Due to the highly exothermic nature of this reaction (the adiabatic decomposition temperature can reach ~1640 °C), the high-temperature stability of catalytic materials is the main challenge for the application of N_2O as a propellant. It has been reported [16] that Ir/Al_2O_3 (Shell 405) had a high activity towards the decomposition of N_2O. However, upon being subjected to the high-temperature treatment (1200 °C), the active components Ir or IrO_2 showed signs of sintering and the alumina support began to irreversibly convert to α-Al_2O_3, thereby drastically reducing the surface area and leading to the activity loss. Therefore, with respect to the thermal stability, many previous catalyst systems used for low concentration N_2O decomposition will not be suitable for high concentration N_2O decomposition, either for the collapse of catalyst structure or the sublimation of active component at high temperatures. A preliminary test on Ni-Co-Zr-O catalyst [16] demonstrated that such a mixed oxide was thermally stable even at 1200 °C, but less active than the shell 405.

Recently, the need for catalysts that remain stable and active over long periods at high operation temperatures—such as energy generation through natural gas combustion, steam reforming and the partial oxidation of hydrocarbons, prompts the rapid development of highly thermal stable catalytic materials. For example, various heat-resistant metal oxides have been tested as catalysts or catalyst supports for the combustion of methane, such as hexaaluminate [17–19],

* Corresponding author. Tel.: +86 411 84379015; fax: +86 411 84691570.
E-mail address: taozhang@dicp.ac.cn (T. Zhang).

0920-5861/$ – see front matter © 2007 Elsevier B.V. All rights reserved.
doi:10.1016/j.cattod.2007.10.093

perovskites [20], or even SiC [21]. Among them, hexaaluminates [22] are considered to be one of the most promising catalysts for this reaction due to their excellent thermal stability and high activity. Moreover, the hexaaluminates can contain catalytically active components in their structures [20,23], thereby inhibiting loss of active component at high temperatures before the structural collapse. In spite of these obvious advantages, most studies on the hexaaluminates so far have been for methane combustion [24–27], whereas their applications to catalytic decomposition of N_2O under severe conditions have been scarcely investigated. In a very recent report, a $BaFeAl_{11}O_{19}$ hexaaluminate catalyst was applied for N_2O abatement in industry but it only showed poor activity [28]. By contrast, we reported Ir-substituted hexaaluminates in our previous communication [29], and found that they were highly active and stable catalysts for N_2O decomposition. In the present work, we made a detailed study on this Ir-substituted hexaaluminates system, with focus on the role played by the framework Ir and Fe in the N_2O decomposition.

2. Experimental

2.1. Catalyst preparation

Ba-Ir-Fe-Al oxide catalysts ($BaIr_xFe_{1-x}Al_{11}O_{19}$, denoted as BIFA-t, t indicates calcination temperature) were prepared by one-pot precipitation [24]. Typically, to prepare $BaIr_{0.2}Fe_{0.8}Al_{11}O_{19}$ ($x = 0.2$), 0.95 g $Ba(NO_3)_2$, 0.90 g 44 wt% H_2IrCl_6, 15.03 g $Al(NO_3)_3{\cdot}9H_2O$ and 1.16 g $Fe(NO_3)_3{\cdot}9H_2O$ were dissolved individually in deionized water at 60 °C, and then mixed together with the pH adjustment with dilute HNO_3 solution to ~1. The resulting mixture solution was then poured with vigorous stirring into a saturated $(NH_4)_2CO_3$ aqueous solution at 60 °C to form the hexaaluminate precursor precipitate. During the precipitation, a large amount of CO_2 was released while the pH value of the solution was maintained between 7.5 and 8.0. The precipitate was aged with continuous stirring in the mother liquor at 60 °C for 3 h followed by filtration and washing with deionized water. The recovered solid was then dried at 120 °C overnight and calcined at 500 °C in air for 2 h. In some cases, further calcinations were conducted at 800, 1000, 1200 or 1400 °C for 4 h in air. For comparison, Ba-Fe-Al (denoted as BFA) and Ba-Ir-Al (denoted as BIA) oxide catalysts were prepared with the same procedure as that for BIFA, without the addition of H_2IrCl_6 or $Fe(NO_3)_3{\cdot}9H_2O$. On the other hand, Ir/Al_2O_3 was prepared by the above precipitation procedure with $Al(NO_3)_3{\cdot}9H_2O$ and H_2IrCl_6 as the starting materials.

2.2. Catalytic activity measurements

Catalytic decomposition of N_2O was carried out in a fixed-bed flow reaction system under atmospheric pressure. 100 mg of a catalyst sample was placed on a quartz filter in the middle part of the quartz reactor. Prior to the reaction, the catalyst sample was pre-reduced with pure H_2 at 400 °C for 2 h. After cooling to room temperature in Ar, the gas flow was switched to the reacting gas mixture containing N_2O (30%, v/v) in Ar at a flow rate 50 ml/min, corresponding to a gas hour space velocity (GHSV) of 30,000 ml/h g. The catalyst temperature was measured using a thermocouple situated close to the catalyst sample. The effluent gas was on-line analyzed by Agilent 6890N gas chromatograph equipped with Chromosorb 103 column and Porapak Q columns. N_2O conversion based on the difference between the inlet and outlet concentration was used as evaluation of the catalytic activity.

2.3. Characterization

The BET specific surface areas were measured by nitrogen adsorption at −196 °C on a Micromeritics ASAP 2010 apparatus. The samples were evacuated firstly at 110 °C for 3 h and then at 350 °C for 5 h prior to their analysis.

Powder X-ray diffraction (XRD) patterns were obtained with a D/Max-βb diffractometer using a Cu Kα radiation source ($\lambda = 0.15432$ nm). The spectra were scanned between $2\theta = 10$–80°. Unit cell parameters were calculated by the least squares method.

Scanning electron microscopy (SEM) experiments were performed with a JSM 6360-LV electron microscope operating at 20–25 kV. The samples were vapor-deposited with gold before analysis.

The actual Ir loadings of the catalysts were determined by Thermo IRIS Interepid II inductively coupled plasma (ICP) after having dissolved solid in a mixture of concentrated acids ($HF + HCl + HNO_3$).

Temperature-programmed reduction of H_2 (H_2-TPR) was performed on a Micromeritics Autochem 2920 apparatus. A 100-mg sample was used for each measurement. The samples were pre-treated in a flow of Ar at 200 °C for 1 h with a heating rate of 10 °C/min. After cooling to 40 °C in Ar, the feed gas was switched to 10% H_2–Ar mixture. Then, temperature was raised from 40 to 900 °C at a rate of 10 °C/min. A thermal conductivity detector (TCD) was used on line for measuring H_2 consumption.

3. Results and discussion

3.1. Evolution of hexaaluminate BIFA

It has been reported [30–32] that the hexaaluminate Ba-Fe-Al oxide could be formed by calcining the corresponding precursor at above 1100 °C. In the present work, we tried to incorporate precious metal Ir into the Ba-Fe-Al oxide mixture. The phase transformation of the Ba-Ir-Fe-Al oxide during the calcination process was monitored by XRD technique. Fig. 1a shows the XRD patterns of the Ba-Ir-Fe-Al oxide with an increase in the calcination temperature. For comparison, the XRD patterns of the Ir/Al_2O_3 calcined at different temperatures are also shown in Fig. 1b. It can be seen that calcining the Ba-Ir-Fe-Al oxide precursor at 500 °C yielded only IrO_2 and γ-Al_2O_3 crystalline phases, no other metal oxides could be detected with XRD, indicating amorphous nature or a highly dispersed state of Ba-Fe oxides on the Al_2O_3 support [23]. The presence of

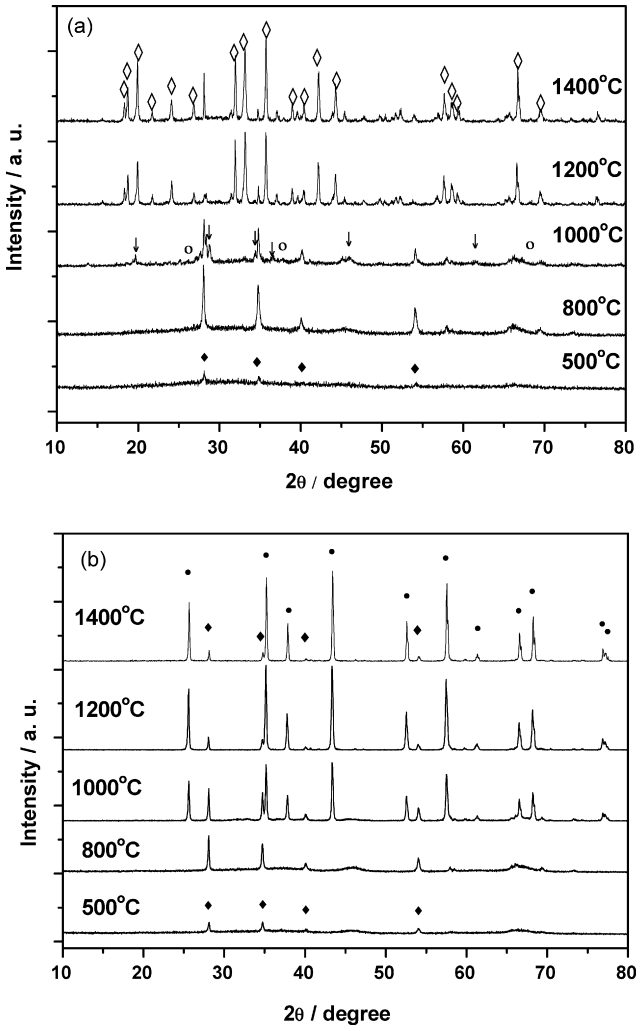

Fig. 1. X-ray diffraction patterns of (a) BIFA catalysts and (b) Ir/Al_2O_3 catalysts. (◆) IrO_2, (◇) $BaAl_{12}O_{19}$, (○) γ-Al_2O_3, (●) α-Al_2O_3 and (↓) $BaAl_2O_4$.

IrO_2 and γ-Al_2O_3 phase was also confirmed by the same XRD patterns of Ir/Al_2O_3-500. It is noted that the sample BIFA-500 has the BET surface area of 215 m^2/g, which is very close to that of Ir/Al_2O_3-500 (see Table 1). Further calcination at 800 °C did not result in marked changes in the XRD patterns except that the intensity of XRD peaks became stronger due to the sintering of IrO_2 particles. The BET surface area of the BIFA-800 was similar to that of Ir/Al_2O_3-800 (around 150 m^2/g), suggesting that the textural properties of the BIFA-800 are still associated with those of the γ-Al_2O_3 matrix. When the Ba-Ir-Fe-Al oxide was calcined at 1000 °C, $BaAl_2O_4$ spinel phase began to appear, accompanied with some decrease in the intensity of IrO_2 peaks, suggesting a part of IrO_2 had been incorporated into the Ba-Fe-Al oxide crystalline phase at this temperature. By contrast, the phase transformation from γ-Al_2O_3 to α-Al_2O_3 occurred on the Ir/Al_2O_3 sample when the calcination was performed at 1000 °C.

A drastic change in the phase composition occurred at 1200 °C. $BaAl_2O_4$ spinel phase disappeared and IrO_2 peaks became weaker. Meanwhile, a new phase corresponding to $BaAl_{12}O_{19}$-type hexaaluminate structure was identified, indicating Ba-Ir-Fe-Al mixed oxide transformed to hexaaluminate and some of the Ir species was incorporated into the hexaaluminate structure. It has been reported [20,23,31] that some transitional metal could be incorporated in hexaaluminate lattice by replacing Al^{3+} cations in tetrahedral or octahedral coordination. In our case, the incorporation of Ir species into the structural lattice of the BFA hexaaluminate could be further confirmed by the change of cell parameters with Ir content. As shown in Table 2, the value of a_0 in the transition metal (both Fe and Ir) incorporated samples is always higher than that of non-substituted $BaAl_{12}O_{19}$. The enlargement of a_0 with an increase in the Ir content confirmed that iridium cations are located in hexaaluminate lattice by replacing Al^{3+} cations. When the BIFA was calcined at 1400 °C, the hexaaluminate structure still retained and the cell parameters of the BIFA-1400 sample remain unchanged, but the IrO_2 peaks became strong again. The intensified IrO_2 peaks were probably caused by the aggregation of IrO_2 particles outsides the hexaaluminate framework. Our ICP analysis indicated that the BIFA-1200 (for $x = 0.2$) had an Ir content of 1.92 wt%, which was higher than that of Ir/Al_2O_3-1200 (1.40 wt%). This result further confirmed that the Ir component in the BIFA had a less mass loss by evaporation than that in the Ir/Al_2O_3 sample during the high-temperature treatment. However, it should be pointed out that the Ir content, either in the BIFA-1200 or in the Ir/Al_2O_3-1200, was significantly lower than the initial value of 5.00 wt% (the value for the sample calcined at 773 K), suggesting that most of the Ir component was lost during the high-temperature treatment. In other words, given that the framework Ir in the hexaaluminate structure could not be lost by evaporation, we can thus think that only a very small part of Ir is incorporated into the hexaaluminate framework.

Table 1
BET surface area and crystalline phase for $BaIr_{0.2}Fe_{0.8}Al_{11}O_{19}$ and Ir/Al_2O_3 catalysts

Catalyst	BET surface area (m^2/g)	Crystalline phase
BIFA-500	215	IrO_2
BIFA-800	159	IrO_2
BIFA-1000	70	IrO_2, $BaAl_2O_4$, γ-Al_2O_3
BIFA-1200	23	IrO_2, $BaAl_{12}O_{19}$
BIFA-1400	10	IrO_2, $BaAl_{12}O_{19}$
Ir/Al_2O_3-500	207	IrO_2, γ-Al_2O_3
Ir/Al_2O_3-1200	6	IrO_2, α-Al_2O_3

Table 2
Cell Parameters of $BaIr_xFe_{1-x}Al_{11}O_{19-\alpha}$

Sample	Cell parameters (Å)	
	$a_0 = b_0$	c_0
$BaIr_{0.8}Fe_{0.2}Al_{11}O_{19}$-1200	5.598	23.029
$BaIr_{0.5}Fe_{0.5}Al_{11}O_{19}$-1200	5.596	22.892
$BaIr_{0.2}Fe_{0.8}Al_{11}O_{19}$-1200	5.582	23.166
$BaAl_{12}O_{19}$-1200	5.576	22.909
$BaIr_{0.2}Fe_{0.8}Al_{11}O_{19}$-1400	5.583	23.094

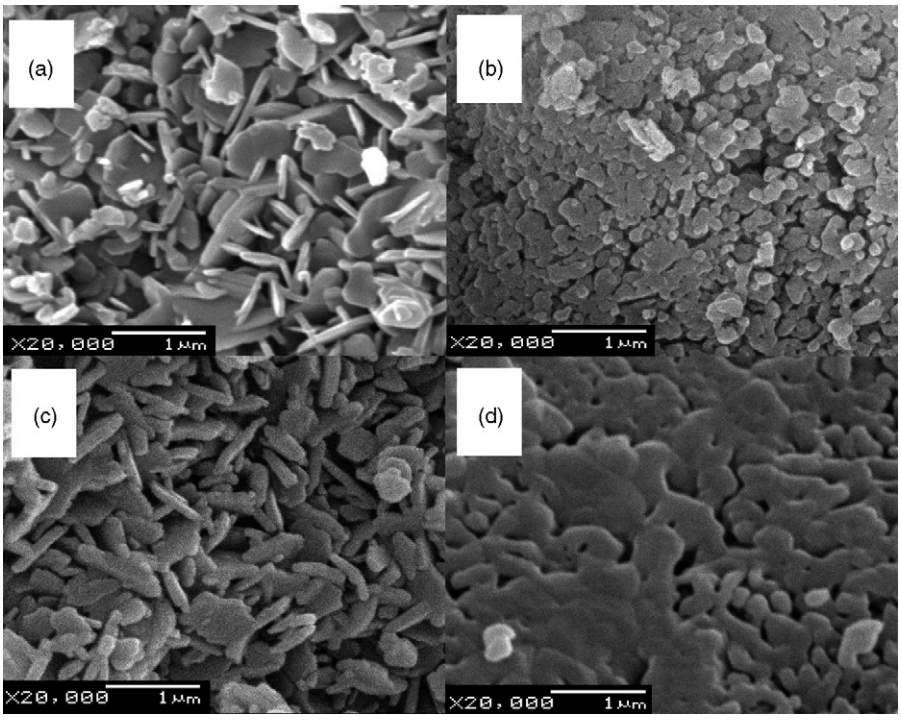

Fig. 2. Scanning electron micrographs of (a) BIFA-1200, (b) Ir/Al_2O_3-1200, (C) BIFA-1400 and (d) Ir/Al_2O_3-1400.

On the other hand, it is noted that the BIFA-1200 had a surface area of 23 m^2/g, almost 4 times larger than that of Ir/Al_2O_3-1200, demonstrating the advantages of hexaaluminates over alumina supported catalysts under high-temperature conditions. This can be further visualized from the SEM images shown in Fig. 2. It is clear that the Ir/Al_2O_3-1200 consists of irregular spherical particles with sizes of ~0.2 μm. After calcination at 1400 °C, extensive sintering can be observed on the Ir/Al_2O_3-1400. Different from the Ir/Al_2O_3, the hexaaluminate BIFA-1200 presents a very uniform plate-like morphology. The thickness of the plates is 20–30 nm. It has been proposed that such peculiar layered structure [33,34] due to anisotropic growth made the hexaaluminate highly resistant to sintering. When the BIFA was calcined at 1400 °C, few changes in the morphology were observed.

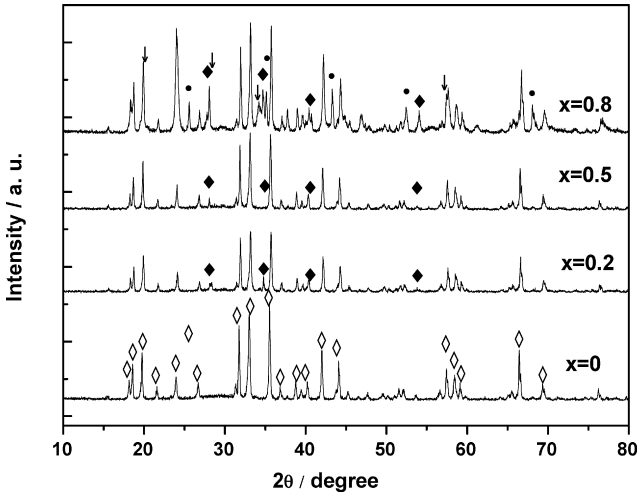

Fig. 3. X-ray diffraction patterns for $BaIr_xFe_{1-x}Al_{11}O_{19}$-1200 catalysts. (◆) IrO_2, (◇) $BaAl_{12}O_{19}$, (●) α-Al_2O_3 and (↓) $BaAl_2O_4$.

3.2. Effect of Ir content on the structure and catalytic performance of BIFA

Fig. 3 illustrates the XRD patters of the $BaIr_xFe_{1-x}Al_{11}O_{19}$-1200 catalysts with different Ir content. For the sample BFA-1200 (i.e., $x = 0$), we can only observe well crystallized hexaaluminate phase. However, for the Ir-containing BIFA samples, the peaks corresponding to the hexaaluminate became a little weak, along with the appearance of the IrO_2 phase. This result suggests that the incorporation of Ir species into the BFA hexaaluminate result in some decrease in the crystallinity. Moreover, with an increase in the x value (Ir content), we can observe more stronger IrO_2 peaks, implying that the excess amount of Ir could not be incorporated into the hexaaluminate structure. In fact, we can see from the cell parameters listed in Table 2 that when the x value increased from 0.5 to 0.8, the a_0 enlargement could be negligible. Accordingly, we prefer to believe that only a very limited amount of Ir has been incorporated into the hexaaluminate structure and contributed to the cell parameter enlargement, while most of the Ir species exist as IrO_2 phase outside the framework and tend to agglomerate during the high-temperature calcination.

Fig. 4 compares the catalytic performances of the $BaIr_xFe_{1-x}Al_{11}O_{19}$ catalysts for the decomposition of high concentration of N_2O. It can be seen that the BFA-1200 (i.e., $x = 0$) which does not contain iridium was almost inactive over the whole investigated temperature range, indicating iridium is the active component. When x increased from 0 to 0.2, the activity increased significantly; the N_2O conversion attained

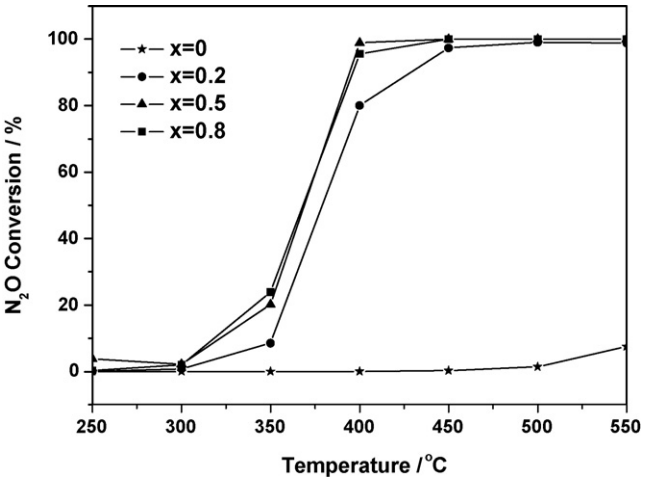

Fig. 4. Effect of Ir content on the catalytic performances over $BaIr_xFe_{1-x}Al_{11}O_{19}$-1200 catalysts.

80% at 400 °C, indicating Ir acts as the main active component for this reaction. With the further increase of Ir content from $x = 0.2$ to 0.5, N_2O conversion increased a little. However, when the Ir content increased from $x = 0.5$ to 0.8, the activity remained unchanged. Such a trend is in accordance with the cell parameter change in Table 2. This result suggests that the large IrO_2 particles which had not been incorporated into the crystalline structure were much less active for N_2O decomposition. Instead, those crystalline framework Ir species were highly active for this reaction.

3.3. Effect of Fe on the Ir-substituted hexaaluminate catalysts

Since the BIFA ($BaIr_xFe_{1-x}Al_{11}O_{19}$) catalysts contain both Ir and Fe components and iridium acts as the active sites in N_2O decomposition, one may ask what a role played by Fe. To answer this question, we attempted to prepare a series of $BaIr_xAl_{12-x}O_{19}$ (BIA) hexaaluminate catalysts without addition of Fe component. Fig. 5 shows the XRD patterns of BIA samples with different x values (i.e., Ir content). It is noted that there appear $BaAl_2O_4$ and α-Al_2O_3 phase besides the hexaaluminate phase. Moreover, with an increase in the Ir content, the diffraction lines due to BIA hexaaluminate phase became weaker, while those corresponding to the $BaAl_2O_4$ and α-Al_2O_3 phase became stronger. This result strongly suggests that it is difficult to obtain pure hexaaluminate without the addition of Fe component, especially under the presence of Ir component. In other words, Fe facilitated the formation of hexaaluminate and the incorporation of Ir into the hexaaluminate framework, although it is inactive by itself for N_2O decomposition.

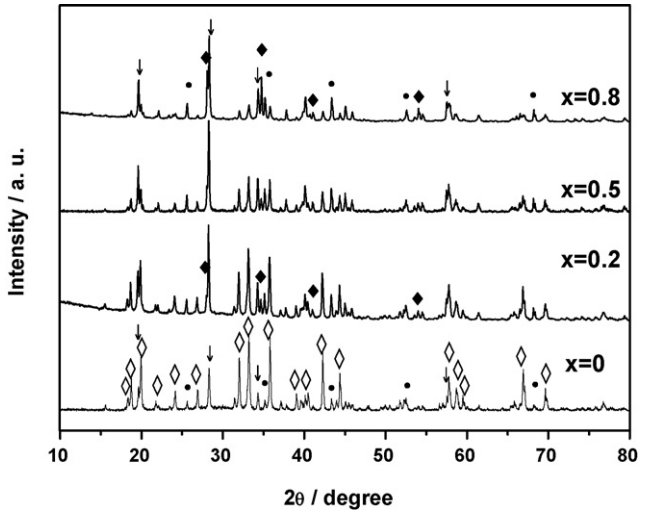

Fig. 5. X-ray diffraction patterns for $BaIr_xAl_{12-x}O_{19}$-1200 catalysts. (◆) IrO_2, (◇) $BaAl_{12}O_{19}$, (●) α-Al_2O_3 and (↓) $BaAl_2O_4$.

3.4. Effect of calcination temperature and pre-treatment atmosphere on the catalytic performances of BIFA

Although the hexaaluminate BIFA was formed at or above 1200 °C, it is very interesting to know whether those oxide precursors are active for N_2O decomposition. Therefore, the effect of calcination temperature on the catalytic activity of BIFA catalyst was investigated. As shown in Fig. 6, BIFA-500 exhibited the best activity for decomposition of high concentration N_2O, which should be attributed to the high dispersion of IrO_2 as shown in XRD (Fig. 1). Compared with BIFA-500, the activity of BIFA-800 decreased slightly. From Table 1 and Fig. 1, we can see that significant sintering occurred on the IrO_2 particles along with the decrease in the specific surface area when the oxide mixture was calcined at 800 °C. Thus, the low activity of the BIFA-800 should be due to the decreased dispersion of active IrO_2 species. The lowest activity was observed on the BIFA-1000 which is associated with the formation of $BaAl_2O_4$ phase. BIFA-1200 exhibited almost the same catalytic activity as BIFA-500. It was worth noting that even after calcination at 1400 °C, the catalyst still showed a similar high activity and was even superior to BIFA-1200 at low reaction temperatures. This result indicates that the structure of Ir-containing hexaaluminate was stable within the investigated

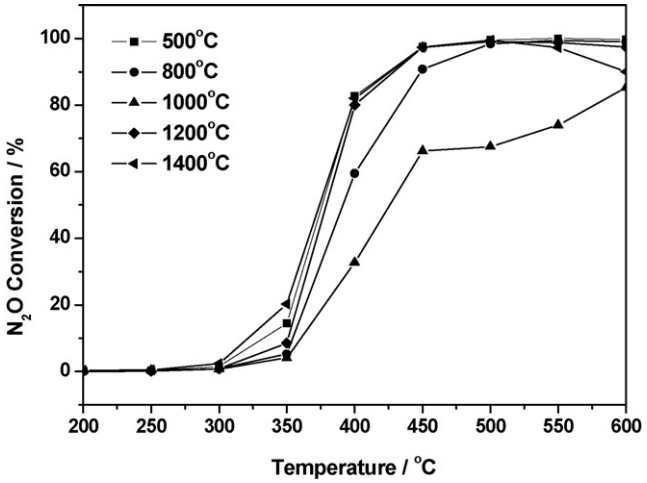

Fig. 6. Effect of calcination temperature on the catalytic performances over BIFA catalysts.

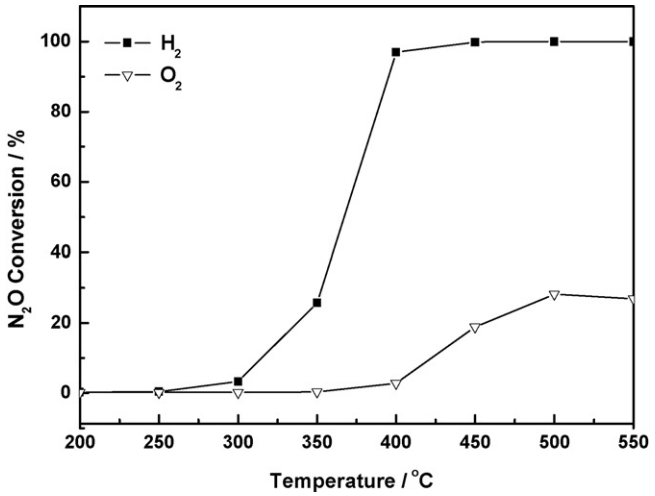

Fig. 7. Effect of pre-treatment conditions on the catalytic activities over BIFA-1200 catalyst.

reaction temperature range and the framework iridium species in the hexaaluminate (BIFA-1200) could be as active as the highly dispersed Ir species in the mixed oxide precursor (BIFA-500).

On the other hand, it was found that the pre-treatment atmosphere imposed a great impact on the catalytic performance of the BIFA catalysts. As shown in Fig. 7, pre-reduction of the BIFA-1200 with pure H_2 at 400 °C yielded high activity, whereas pre-treatment with O_2 resulted in very poor performance. To know what changes occurring during the reduction pre-treatment, temperature-programmed reduction with H_2 (H_2-TPR) was conducted on the samples which had been calcined at different temperatures (Fig. 8). For the BIFA-500, the two reduction peaks, a major one at ~160 °C and a minor one at ~220 °C, could be assigned to the reduction of IrO_2 to metallic Ir. The amount of hydrogen consumption summarized in Table 3 shows that about 1.8×10^{-4} mol/g of Ir^{4+} were reduced to metallic Ir, which is in agreement with the

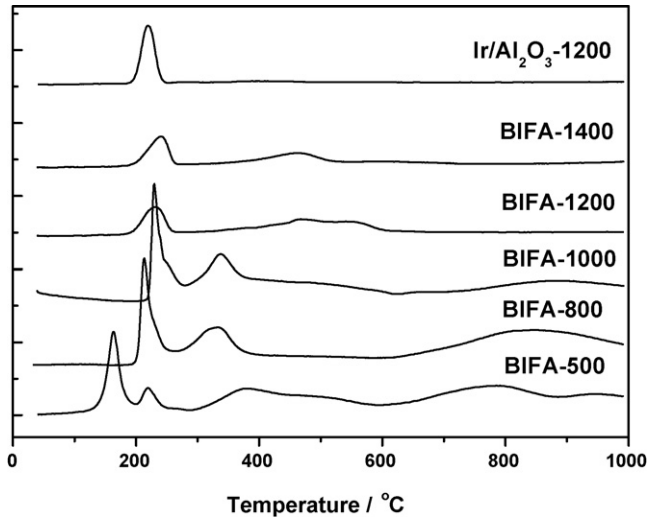

Fig. 8. TPR profiles for BIFA and Ir/Al_2O_3 catalysts calcined at different temperatures.

actual Ir content (2.2×10^{-4} mol/g) in the sample. The presence of the two reduction peaks might be caused by the reduction of IrO_x particles with different particle sizes [35,36]. Besides the reduction peaks of IrO_2, the peaks at temperatures above 300 °C assignable to the reduction of Fe^{3+} [37] could also be observed.

It is noted that with an increase in the calcination temperature (until 1000 °C), the major reduction peak of IrO_2 shifted to a higher temperature and the minor reduction peak became undistinguishable with the major peak. From the XRD examinations (Fig. 1) we know that IrO_2 particles became larger with the calcination temperature rise. According to literature [36], the large IrO_2 particles were more difficult to be reduced than the small ones. Therefore, sintering or agglomeration occurring during the high-temperature calcination would make the original small IrO_2 particles become large, leading to their reduction peak shifting to a higher temperature and overlapping with the second IrO_2 reduction peak. Meanwhile, there appeared a new peak at ~335 °C, which should be caused by the partial reduction of $Fe^{3+} \rightarrow Fe^{2+}$. It was reported [38,39] that noble metals could facilitate the reduction of the transition metal oxides via spillover of hydrogen. With the calcination temperature rise, the Ir oxides may interact more strongly with the iron oxides, thus improve the spillover of H_2 and make the iron oxides more reducible. From Table 3, we can see that the amount of H_2 consumed for reducing $Fe^{3+} \rightarrow Fe^{2+}$ is 3.7×10^{-4} mol/g on the BIFA-800 and 4.8×10^{-4} mol/g on the BIFA-1000, respectively, which well accords with the theoretical value of 4.1×10^{-4} mol/g within the calculation error.

When the sample was calcined at 1200 °C, its TPR profile appears very different. The reduction peak of IrO_2 decreased sharply in the intensity. This was caused by the two possible reasons. On one hand, a significant loss of iridium occurred when the sample was calcined at 1200 °C, as indicated by our ICP analysis. On the other hand, a small amount of Ir was incorporated into the hexaaluminate framework and could not be reduced at this temperature, while only large IrO_2 particles outside the framework could be reduced. The two changes contributed together to the lowering in intensity of IrO_2 reduction peak. It is noted that upon formation of hexaaluminate, the reduction of Fe^{3+} became more difficult, as indicated by its TPR peak shifting to a higher temperature. This should also be caused by the incorporation of Fe^{3+} into the hexaaluminate framework [40]. With a further increase in the calcination temperature to 1400 °C, little changes have been observed on the TPR profile due to the stability of the hexaaluminate structure. Since there were more IrO_2 particles on the Ir/Al_2O_3-1200 than those on the BIFA-1200, the Ir/Al_2O_3-1200 presented a slightly larger reduction peak of IrO_x at ca. 220 °C.

In summary, from the above TPR results together with the catalytic performance, we can conclude that the highly dispersed metallic Ir species, either in the BIFA-500 or in the Ir/Al_2O_3-500, is active for the N_2O decomposition, whereas the large Ir particles in the BIFA-800, BIFA-1000 and Ir/Al_2O_3-1200, are much less active. On the other hand, the Ir species in

Table 3
Summarizing data for TPR experiments on BIFA ($x = 0.2$) and Ir/Al_2O_3 samples

Samples	Peak position (°C)	Amount of H_2 consumed (mol/g)	Ir moles reduced (mol/g)	Fe moles reduced (mol/g)
BIFA-500	163.5	2.7×10^{-4}	1.8×10^{-4}	
	219.2	8.5×10^{-5}		
	379.8	3.7×10^{-4}		7.4×10^{-4}
BIFA-800	213.3	2.9×10^{-4}	1.4×10^{-4}	
	334.2	3.7×10^{-4}		7.3×10^{-4}
BIFA-1000	229.4	3.0×10^{-4}	1.5×10^{-4}	
	337.6	4.8×10^{-4}		9.5×10^{-4}
BIFA-1200	226.7	1.3×10^{-4}	6.3×10^{-5}	
	458.0	3.9×10^{-4}		7.8×10^{-4}
BIFA-1400	239.9	1.4×10^{-4}	6.9×10^{-5}	
	462.6	2.1×10^{-4}		4.1×10^{-4}
Ir/Al_2O_3-1200	219.0	1.7×10^{-4}	8.7×10^{-5}	

the hexaaluminate framework of BIFA-1200 sample, in spite of in its oxidation state, is as active as those highly dispersed metallic Ir species.

3.5. Comparison of catalytic performances between BIFA and Ir/Al_2O_3

Fig. 9 showed N_2O conversions as a function of reaction temperature over various hexaaluminates and Ir/Al_2O_3 catalysts. It can be seen that the BIFA-500 exhibited only slightly higher activity than the Ir/Al_2O_3-500 for high concentration N_2O decomposition. At a reaction temperature of 400 °C, N_2O conversion was 93% over the BIFA-500, while it was 91% for the Ir/Al_2O_3-500. However, when the catalysts were calcined at 1200 °C for 4 h, the activity difference between the BIFA and Ir/Al_2O_3 became remarkable. The BIFA-1200 still showed a high activity, with the N_2O conversion of 80.1% at 400 °C, which was only 13% lower than that of BIFA-500. In contrast, Ir/Al_2O_3-1200 demonstrated rather low activity, the N_2O conversion was only 3.3% at 400 °C. The results clearly demonstrate that the hexaaluminate BIFA is much superior to Ir/Al_2O_3 under high-temperature conditions. The high activity of the BIFA should have a close relation with its textural properties. As shown in Table 1, the surface areas of both the BIFA and the Ir/Al_2O_3 which had been calcined at 500 °C were around 210 m^2/g, and they decreased dramatically with increasing the calcination temperatures. However, the BET surface area of BIFA-1200 was 23 m^2/g, which was 4 times larger than that of the Ir/Al_2O_3-1200. Hence, the high surface area of the BIFA-1200 catalyst could be one reason for its high activity.

Not only with the high activity, the BIFA catalyst also had a high thermal stability. In order to assess the short-term stability of the catalysts, the N_2O conversion was monitored with the time on stream, as illustrated in Fig. 10. It can be seen that with the prolonging of the reaction time at 450 °C, both catalysts exhibited activity decay. However, the activity decay over the Ir/Al_2O_3-1200 became more rapidly with the extending of reaction time. In particular, when the reaction time was

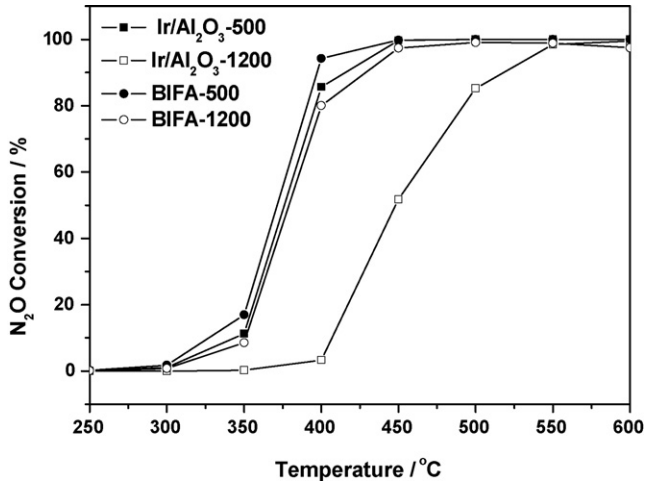

Fig. 9. Comparison between catalytic activities over BIFA and Ir/Al_2O_3 catalysts.

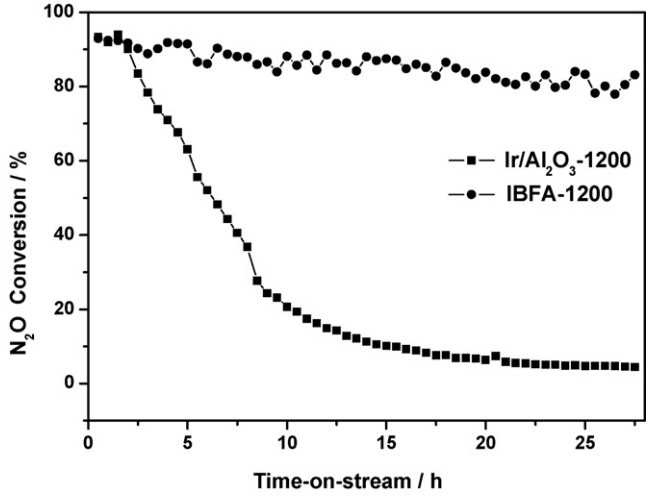

Fig. 10. Evolution of N_2O conversions at 450 °C as a function of the time-on-stream over BIFA-1200 and Ir/Al_2O_3-1200 catalysts.

prolonged to 10 h, N_2O conversion at 450 °C over the Ir/Al_2O_3 declined from 91% to 20%, whereas it only slightly decreased from 100% to 90% over the BIFA catalyst, strongly demonstrating the outstanding advantage of the BIFA over Ir/Al_2O_3 under react condition. Moreover, BIFA-1200 could retain ~90% N_2O conversion at 450 °C for more than 26 h without visible decay, in contrast with the rapid decay to naught over the Ir/Al_2O_3-1200. This result further demonstrated that Ba-Ir-Fe-Al catalyst had the ability to sustain the catalytic activity compared to that of Ir/Al_2O_3. It is known that the thermal stability of catalyst materials is a key factor to influence the application of high concentration of N_2O as a propellant [14]. Therefore, our highly active and thermally stable BIFA catalysts will find widespread applications in aircraft propulsion systems.

4. Conclusion

The Ir-substituted hexaaluminate, which showed high activity and excellent thermal stability for N_2O decomposition has been successfully synthesized by one-pot precipitation procedure. The iridium was incorporated into the hexaaluminate lattice by substituting Al^{3+} after being calcined at 1200 °C. Such incorporated Ir species in the hexaaluminate structure is responsible for the high activity of the catalyst, whereas those Ir species outside the hexaaluminate crystalline framework are susceptible to sintering and less active for this reaction. The addition of Fe component facilitated the formation of hexaaluminate and the incorporation of Ir into the hexaaluminate framework. The much higher activity and stability of the BIFA than that of the Ir/Al_2O_3 at high-temperature conditions indicates the Ir-substituted hexaaluminate is a promising catalyst towards high concentration nitrous oxide decomposition for space applications.

Acknowledgements

Supports of National Science Foundation of China (NSFC) for Distinguished Young Scholars (No. 20325620) and NSFC grant (Nos. 20673116 and 20773122) are gratefully acknowledged.

References

[1] F. Kapteijn, J.R. Mirasol, J.A. Moulijn, Appl. Catal. B 9 (1996) 25.
[2] V.K. Tzitzios, V. Georgakilas, Chemosphere 59 (2005) 887.
[3] K. Doi, Y.Y. Wu, R. Takeda, A. Matsunami, N. Arai, T. Tagawa, S. Goto, Appl. Catal. B 35 (2001) 43.
[4] L. Yan, T. Ren, X.L. Wang, D. Ji, J.H. Suo, Appl. Catal. B 45 (2003) 85.
[5] L. Yan, X.M. Zhang, T. Ren, H.P. Zhang, X.L. Wang, J.H. Suo, Chem. Commun. (2002) 860.
[6] S. Kannan, Appl. Clay Sci. 13 (1998) 347.
[7] L. Obalová, K. Jirátová, F. Kovanda, K. Pacultová, Z. Lacný, Z. Mikulová, Appl. Catal. B 60 (2005) 297.
[8] L. Obalová, K. Jirátová, F. Kovanda, M. Valásková, J. Balabánová, K. Pacultová, J. Mol. Catal. A 248 (2006) 210.
[9] L. Obalová, K. Pacultová, J. Balabánová, K. Jirátová, Z. Bastl, M. Valášková, Z. Lacný, F. Kovanda, Catal. Today 119 (2007) 233.
[10] J. Haber, T. Machej, J. Janas, M. Nattich, Catal. Today 90 (2004) 15.
[11] B.R. Wood, J.A. Reimer, A.T. Bell, M.T. Janicke, K.C. Ott, J. Catal. 224 (2004) 148.
[12] M. Cabrera, F. Kapteijn, J.A. Moulijn, Chem. Commun. (2005) 2178.
[13] V. Zakirov, T.J. Lawrence, J.J. Sellers, M.N. Sweeting, in: Proceedings of the 5th International Symposium on Small Satellite Systems and Services, France, (2000), p. 19.
[14] V. Zakirov, V. Goeman, T.J. Lawrence, M.N. Sweeting, in: Proceedings of the 14th Annual AIAA/USU Conference on Small Satellite, The United States, (2000), p. 21.
[15] V. Zakirov, T.J. Lawrence, J.J. Sellers, M.N. Sweeting, in: Proceedings of the 51th International Astronautical Congress, Rio de Janeiro, Brazil, (2000), p. 2.
[16] J.R. Wallbank, P.A. Sermon, A.M. Baker, L. Courtney, R.M. Sambrook, The 2nd International Conference on Green Propellants for Space Propulsion, 2004, p. 7.
[17] H. Inoue, K. Sekizawa, K. Eguchi, H. Arai, Catal. Today 47 (1999) 181.
[18] M. Machida, K. Eguchi, H. Arai, J. Catal. 103 (1987) 385.
[19] M. Machida, K. Eguchi, H. Arai, J. Catal. 123 (1990) 477.
[20] T. Utaka, S.A. Al-Drees, J. Ueda, Y. Iwasa, T. Takeguchi, R. Kikuchi, K. Eguchi, Appl. Catal. A 247 (2003) 125.
[21] T. Okutani, Y. Nakata, M. Suzuki, H. Nagai, Catal. Today 26 (1995) 247.
[22] N. Iyi, S. Takekawa, S. Kimura, J. Solid State Chem. 83 (1989) 8.
[23] G. Groppi, C. Cristiani, P. Forzatti, Appl. Catal. B 35 (2001) 137.
[24] B.W.-L. Jang, R.M. Nelson, J.J. Spivey, M. Ocal, R. Oukaci, G. Marcelin, Catal. Today 47 (1999) 103.
[25] J.C. Sung, S.S. Yong, S.S. Kwang, J.J. Nam, K.K. Sung, Appl. Catal. B 30 (2001) 351.
[26] H. Arai, M. Machida, Appl. Catal. A 138 (1996) 161.
[27] G. Groppi, C. Cristiani, P. Forzatti, J. Catal. 168 (1997) 95.
[28] J.P. Ramírez, M. Santiago, Chem. Commun. (2007) 619.
[29] S.M. Zhu, X.D. Wang, A.Q. Wang, Y. Cong, T. Zhang, Chem. Commun. (2007) 1695.
[30] L. Lietti, C. Cristiani, G. Groppi, P. Forzatti, Catal. Today 59 (2000) 191.
[31] R. Kikuchi, Y. Iwasa, T. Takeguchi, K. Eguchi, Appl. Catal. A 281 (2005) 61.
[32] M. Machida, K. Eguchi, H. Arai, J. Catal. 120 (1989) 377.
[33] A.J. Zarur, J.Y. Ying, Nature 403 (2000) 65.
[34] A.J. Zarur, H.H. Hwu, J.Y. Ying, Langmuir 16 (2000) 3042.
[35] C. Carnevillier, F. Epron, P. Marecot, Appl. Catal. A 275 (2004) 25.
[36] P. Reyes, M.C. Aguirre, G. Pecchi, J.L.G. Fierro, J. Mol. Catal. A 164 (2000) 245.
[37] A. Venugopal, M.S. Scurrell, Appl. Catal. A 258 (2004) 241.
[38] V. Boissel, S. Tahir, C.A. Koh, Appl. Catal. B 64 (2006) 234.
[39] G. Jacobs, T.K. Das, Y. Zhang, J. Li, G. Racoillet, B.H. Davis, Appl. Catal. A 233 (2002) 263.
[40] P.A. Duart, J.M. Millet, N. Guilhaume, E. Garbowsik, M. Primet, Catal. Today 59 (2000) 163.